International Journal of Minerals, Metallurgy and Materials
Volume 29, Number 7, July 2022, Page 1343
https://doi.org/10.1007/s12613-021-2370-7

Enhanced mechanical properties of Mg–3Al–1Zn alloy sheets through slope extrusion

Huabao Yang[1)], *Yanfu Chai*[1,2),✉], *Bin Jiang*[3),✉], *Chao He*[3)], *Junjie He*[4)], *Qingshan Yang*[5)], *and Ming Yuan*[3)]

1) School of Mechanical and Electrical Engineering, Shaoxing University, Shaoxing 312000, China
2) Tianjin Key Laboratory of Composite & Functional Materials, School of Materials Science and Engineering, Tianjin University, Tianjin 300072, China
3) State Key Laboratory of Mechanical Transmissions, College of Materials Science and Engineering, Chongqing University, Chongqing 400044, China
4) College of Materials Science and Engineering, Yunnan University, Kunming 650091, China
5) School of Metallurgy and Material Engineering, Chongqing University of Science and Technology, Chongqing 401331, China
(Received: 11 September 2021; revised: 27 October 2021; accepted: 27 October 2021)

Abstract: A novel extrusion approach, entitled slope extrusion (SE), was employed to manufacture AZ31 (Mg–3Al–1Zn, wt%) alloy sheets. The microstructures, textures, and mechanical properties were investigated, compared with those of the AZ31 sheet fabricated by conventional extrusion (CE). Through the combination of finite element simulation and actual experiment, the ultimate results indicated that significant grain refinement (from 9.1 to 7.7 and 5.6 μm) and strong basal texture (from 12.6 to 17.6 and 19.5 mrd) were achieved by the SE process. The essence was associated with the additional introduced inclined interface in the process of SE, which could bring about more asymmetric deformation and stronger accumulated strain along the ND when compared with the process of CE. As a consequence, the SE sheets exhibited a higher yield strength (YS) and ultimate tensile strength (UTS) than the counterparts of the CE sheet, which was mainly assigned to the synergistic effects from grain refining and texture strengthening.

Keywords: AZ31 Mg alloy sheets; slope extrusion; microstructure; texture; strength

1. Introduction

As one of the lightest metal structural materials, magnesium (Mg) and its alloys have attracted remarkable attention in automotive, aerospace, and other industries [1–2]. However, up to date, the low absolute strength is a major bottleneck for the widespread application of Mg alloys in structural materials. As well known, grain refinement is deemed as an effective approach to upgrade the strength of Mg alloys, due to a large K value [3–4]. However, at present the grain size of as-cast Mg alloy is relatively bulky, and which ultimately give rise to a low strength performance. Therefore, various severe plastic processing technologies [5–7], such as extrusion [8–10], forging [11], and rolling [12], have been dedicated to achieve the goal of grain refinement and then significantly improve the strength and plastic of the Mg alloys. Unfortunately, it must be admitted that the plastic processed Mg alloys normally have a certain texture, such as a basal texture of conventional extruded AZ31 (Mg–3Al–1Zn, wt%) alloy sheet [13]. Originating from the fact that both the plastic deformation behavior and mechanical properties of Mg alloys are very sensitive to the crystallographic texture, texture control is regarded as an effective method to optimize the mechanical properties of Mg alloys [14]. In particular, reasonable texture enhancement contributes to improve the strength of Mg alloys, albeit it may sacrifice some plasticity. In general, strength and plasticity are not compatible. However, when the grain refinement in combination with the texture reinforcement, the strength of Mg alloy sheet can be effectively increased and not at the expense of a severe deterioration in plasticity. Such as, during the high-ratio differential speed rolling (HRDSR) process [15], the grain refining can be achieved by the continuous dynamic recrystallization, and eventually ultra-fine grained AZ31 shows a relatively large post-uniform elongation. Meanwhile, the enormous strain in large strain rolling (LSR) [16] causes the significant grain refinement. Especially, after only one pass with 80% reductions, the strength increases dramatically and the ductility kept constant.

Extrusion technology is one of the economic processes to produce the Mg alloy plate [17–18]. In recent years, extensive work has been employed to improve the mechanical properties of Mg alloys via controlling the extrusion process parameters [19–20], the design optimization of extrusion die [21], and so on. But these jobs not only take a long period, but also cost a lot. Therefore, it is urgent to explore a simple and effective extrusion approach to improve the mechanical properties of Mg alloy.

In our present research, a novel extrusion approach entitled slope extrusion (SE) was employed to produce AZ31 alloy sheets. With more details, AZ31 alloy ingots were split into two unequal pieces along the specific path before the ex-

✉ Corresponding authors: Yanfu Chai E-mail: 1073330140@qq.com; Bin Jiang E-mail: Jiangbinrong@cqu.edu.cn

trusion. As a result, through detailed observation of the microstructure, texture, and rheological behavior, it can be concluded that slope extrusion can significantly improve the strength of Mg alloy sheet. Such an investigation carried out an important attempt for the significant improvement of strength in AZ31 alloy sheet, which may further accelerate their practical application. In addition, the impact of designed inclined interface on the deformation behavior unveiled in this research could provide guidance for the development of similar Mg alloys in the future.

2. Experimental

The commercial AZ31 cast ingots with 80 mm in diameter and 60 mm in length were homogenized at 400°C for 12 h and then cooled in air prior to extrusion. Subsequently, three different types of sheets with 3 mm in thickness and 60 mm in width were extruded at 400°C under the extrusion ratio of 32:1. Schematic diagrams for the fabrication of the CE and SE sheets are presented in Fig. 1. As shown in Fig. 1, two SE sheets were obtained from two slope extrusion processes, respectively. One process is considered as the slope extrusion I (nominated as SE1), and the other one was entitled as the slope extrusion II (nominated as SE2). In SE1, the whole ingot was cut into two unequal pieces along a diagonal which tilted away from the axis direction. Then, two pieces were bundled into a complete ingot for the following extrusion. In SE2, the ingot was split into two unequal pieces along a wavy line. Subsequently, these pieces were tied up as a whole for the subsequent extrusion.

The microstructure was characterized by optical microscopy (OM), and the average grain size was measured by a linear intercept method. Electron backscatter diffraction (EBSD) measurements were conducted in the extruded direction (ED)–normal direction (ND) plane of the various samples at 20 kV and the corresponding scan step was set as 0.6 μm. Furthermore, in order to verify the phenomenon of texture strengthening caused by the slope extrusion, the macro-texture measurements were also performed on the top surface of three sheets by using X-ray diffraction (XRD, Rigaku D/Max 2500) with Cu K_α radiation. The tensile tests were carried out at room temperature with an initial strain rate of 10^{-3} s^{-1} by using CMT6305-300KN testing machine and each sheet was repeated three times to confirm the consistency of results. Each sample was machined from their respective sheets along the ED, had a gauge length of 14 mm, a width of 6 mm, and a thickness of 3 mm.

3. Results and discussion

3.1. Simulation results

As shown in Fig. 2, a finite element model was employed to simulate the processes of CE and SE. In this simulation model, the type of work piece is set as plastic, while others such as the top and bottom dies are rigid. The velocity of the top die is set as 3 mm/s. Ultimately, at the stage of post-deformation, the state variable between two points is used to analyze the strain evolution in the red zone (seen in Fig. 2), and the point tracking is also adopted to describe the stress in the black dot (seen in Fig. 2).

The strain and stress evolution along the ND of the CE, SE1 and SE2 sheets are shown in Fig. 3. Fig. 3(a) describes the distribution of effective strain along the ND in the red zone, representing the incipient extrusion channel for the sheet forming. The distribution of normal strain for the CE sheet along the ND is changeless, while it presents a great fluctuation in the processes of SE1 and SE2. As shown in Fig. 3(b), it can be found that the normal stress begins to drop dramatically when the work piece enters into the severely deformed region. Besides, the normal compressive stresses in the SE1 and SE2 sheets are considerably larger than the counterparts of CE sheet. The above phenomenon indicates

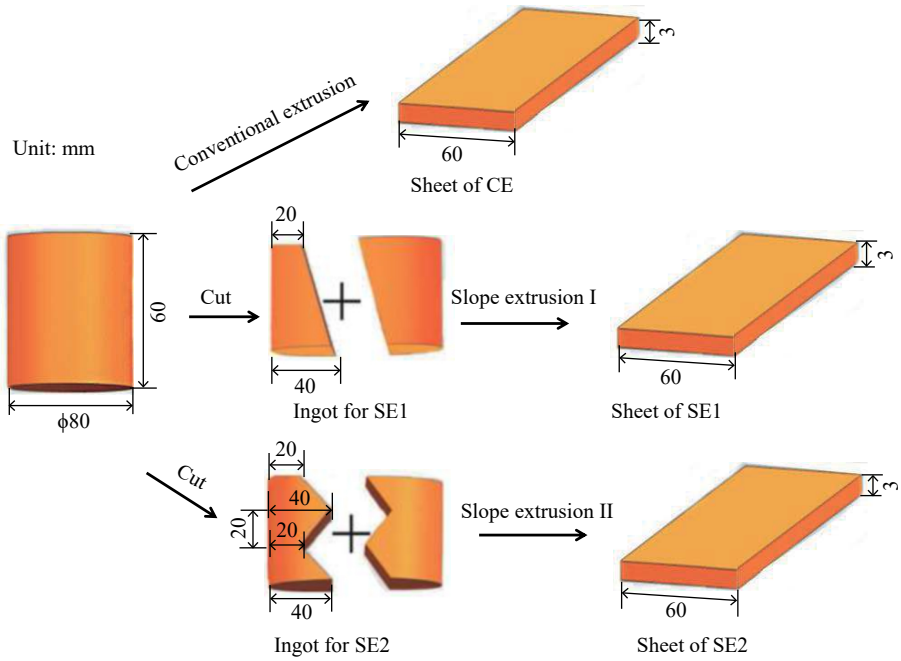

Fig. 1. Schematic diagrams for the fabrication of the CE and SE sheets.

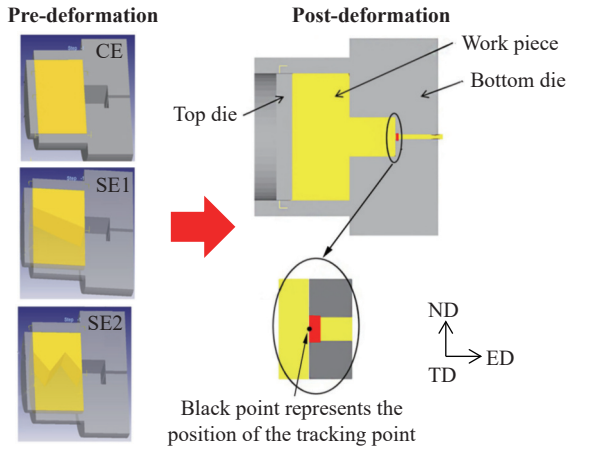

Fig. 2. Schematic diagrams of CE and SE sheets at the stage of pre-deformation during the finite element simulation (left) and the tracking position for stress–strain state at the state of post-deformation (right).

that a larger strain gradient along the ND is formed during the slope extrusion via the introduction of an inclined interface. The essence is ascribed to asymmetric deformation and mutual friction between the block and block. Hence, it is reasonably speculated that, compared with the conventional extrusion, the additional introduced inclined interface in the process of slope extrusion would bring about more asymmetric deformation and stronger accumulated strain along the ND.

3.2. Microstructural evolution

Optical micrographs along with the distribution of grain size obtained from the ED–ND plane of the CE, SE1, and SE2 samples are presented in Fig. 4. For the CE sample, the microstructure is heterogeneous, occupied by a certain number of large elongated, deformed grains of 14–18 μm along with fine recrystallized grains of 1.5–2.7 μm. In contrast, after the slope extrusion, it is evident that the above mentioned coarse and elongated deformed grains are significantly reduced and replaced by a notable increase in the proportion of fine recrystallized grains, which eventually contributes to the improvement of microstructural uniformly. Furthermore, the average grain size of SE1 and SE2 samples is 7.7 and 5.6 μm, respectively, which is much finer than that of the CE sample (9.1 μm). Therefore, it can be concluded that the application of SE process is conductive to the significant grain refinement and homogeneous microstructure, compared with the CE process. The possible reason for the above phenomena can be attributed to the generation of a bigger strain gradient along the ND of sheets during the SE process. Lu *et al*. [22] also reported that the distribution and inhomogeneity of equivalent strain play an important role in grain refinement. Meanwhile, Yang *et al*. [23] suggested that the top surface of the asymmetric extruded sample is imposed to larger effective strain by the interaction between the container and the surface during the extrusion process than that of the sample at the mid-layer, leading to grain refinement. Hence, significant grain refinement exists in the SE sheets are pertaining to the increased strain gradient, which resulted from the role in the tilted interface during the SE processes.

As shown in Fig. 5, the inverse pole figure (IPF) map of the CE, SE1, and SE2 samples all contain the majority of red grains and a small number of grains with other colors. Besides, after the slope extrusion, the intensity of basal micro-texture in SE1 and SE2 samples presents a relatively higher value, 17.6 and 19.5 mrd, respectively, compared with that of the CE sample (12.6 mrd). Both of them indicate that the significant texture strengthening is achieved by the SE processes.

The (0002) pole figures obtained from the CE, SE1, and SE2 samples by XRD measurements are shown in Fig. 6. For the CE sample, its basal pole slightly rotates away from the center of the (0002) pole figure. Comparatively speaking, for the SE1 and SE2 samples, the *c*-axis of grains is almost parallel to the ND and accompanied by a stronger texture intensity of 19.7 and 25.4 mrd, respectively, than that of the CE sample (11.4 mrd). The above results (a good matching correspondence between macro-texture and micro-texture) once again confirm that the SE processes will lead to the enhancement basal texture.

Fig. 7 reveals the recrystallization degree of the AZ31 alloy fabricated by three different extrusion processes. It can be found that the volume fraction of red-deformed grains is gradually decreased from the CE to SE1 and SE2 processes (from 15.7% to 12.6% and 9.3%), which implies that in the process of hot extrusion, the degree of recrystallization in the SE sheets is immensely higher than that in the CE sheet.

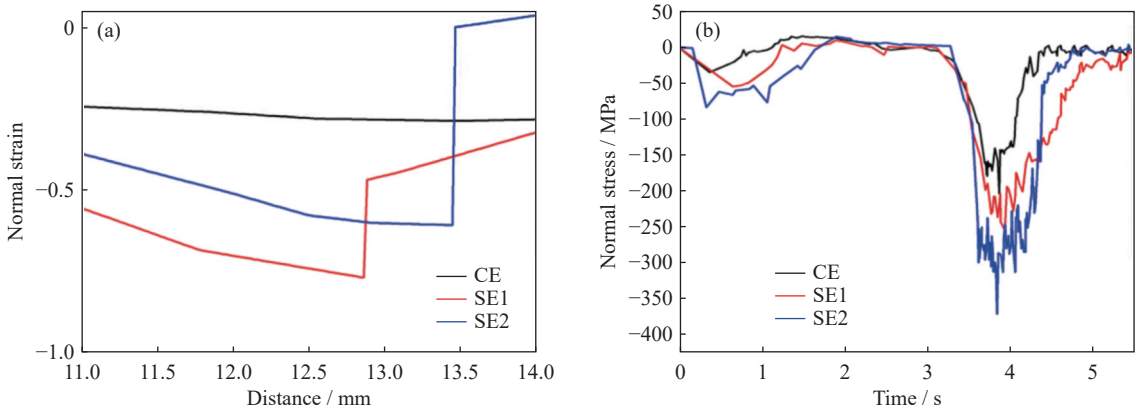

Fig. 3. Effective strain of the tracked points (the red zone in Fig. 2) (a) and the effective stress (the black dot in Fig. 2) (b) along ND of the AZ31 work piece during the finite element models in the extrusion process, which is corresponding to the black dot in Fig. 2.

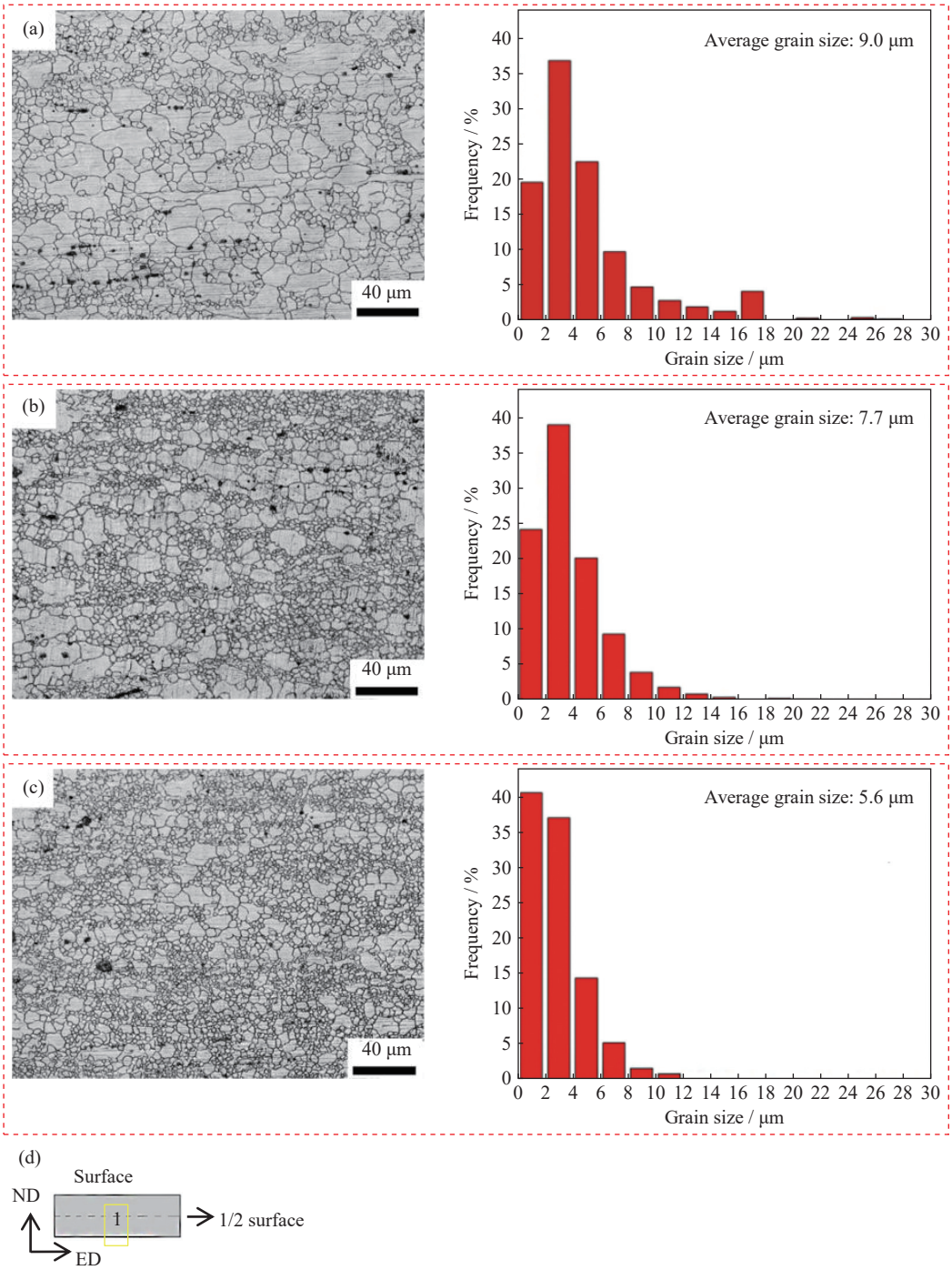

Fig. 4. Optical microstructures and summary of grain size distribution (right) in different sheets: (a) CE; (b) SE1; (c) SE2. (d) shows the region of the sheet for OM analysis, i.e., the yellow square frame in (d).

As a result, in conjunction with the Figs. 6 and 7, it reflects that the SE processes can not only induce the texture strengthening, but also accelerate the degree of dynamic recrystallization. The above phenomenon may be linked to the modified stress state (intensified normal strain) during the extrusion. As shown in Fig. 3, the relevant simulation results clearly reveal that there exists a stronger strain along the ND of the sheet during the SE processes, which will inevitably give rise to a difficulty of the rotation of the basal plane and then contributes to basal texture enhancement. Similarly, Wu *et al*. [24] also expressed that the texture of Mg–3Gd–1Zn alloy is enhanced during the process of cold rolling through enhanced normal strain.

3.3. Mechanical behavior

True stress–true strain relations at room temperature obtained from the CE, SE1, and SE2 sheets along the ED are demonstrated in Fig. 8(a). Related average values for yield strength (YS), ultimate tensile strength (UTS), and elongation-to-failure (EL) for the CE, SE1, and SE2 sheets are calculated and presented in Fig. 8(b). The YS of SE1 and SE2 sheets (191.1 MPa and 219.7 MPa, respectively) are both much higher than that of the CE sheet (177.6 MPa). The UTS exhibits a rising trend from CE to SE1 and SE2 sheets (from

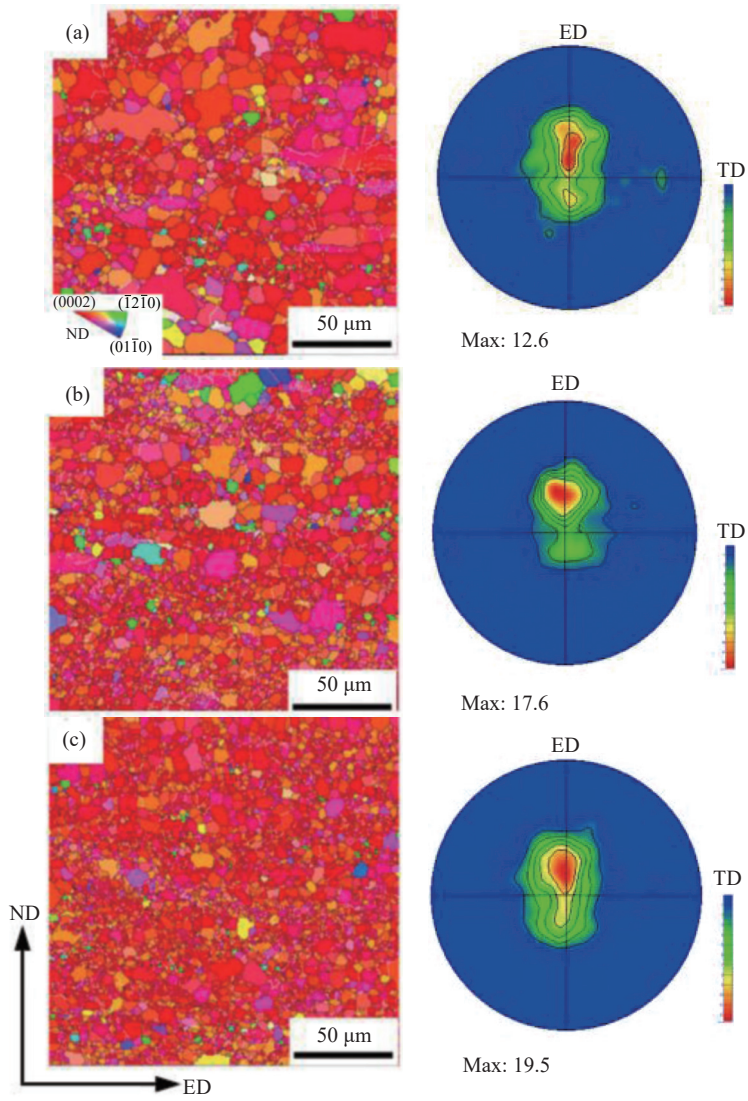

Fig. 5. Inverse pole figure map and (0002) pole figures of specimens which subjected to multiple different extrusion process: (a) CE, (b) SE1, and (c) SE2. TD is transverse direction; Max is the maximum intensity.

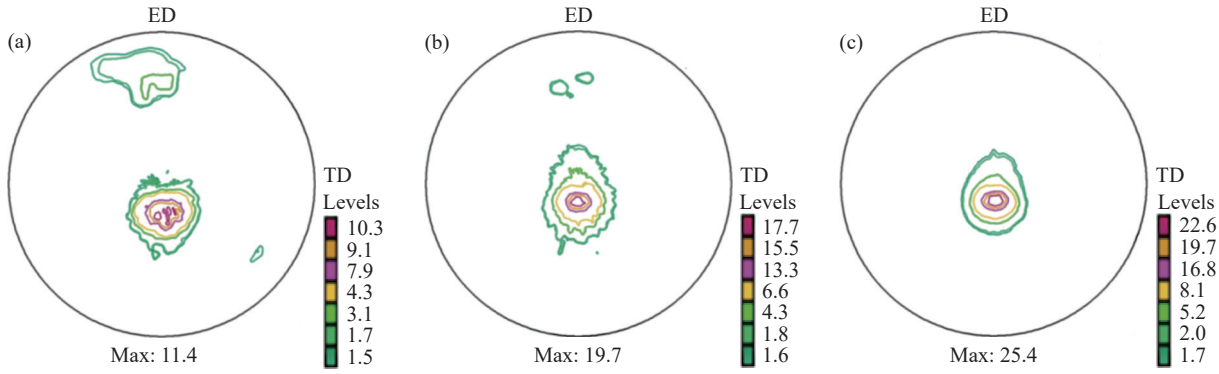

Fig. 6. (0002) pole figures of three samples by the way of XRD: (a) CE sheet; (b) SE1 sheet; (c) SE2 sheet.

392.9 to 394.4 and 410.7 MPa). Hence, compared with the CE sheet, SE sheets possess the higher values of YS and UTS. The possible cause is associated with the fine grain size and high basal texture intensity. In general, the effect of grain boundary strengthening can be described via the Hall-Petch equation as follow:

$$\sigma_y = \sigma_0 + kd^{-1/2} \tag{1}$$

where σ_y is the yield strength; d is the average grain size; both k and σ_0 are texture dependent, where k is the Hall-Petch coefficient (220 MPa·μm$^{1/2}$ for the Mg alloys with typical basal texture [25]), and σ_0 is the friction stress for dislocation movement and is given as follow [26]:

$$\sigma_0 = m\tau_0 \tag{2}$$

where m is the Taylor factor (approximately 6.5 times of the

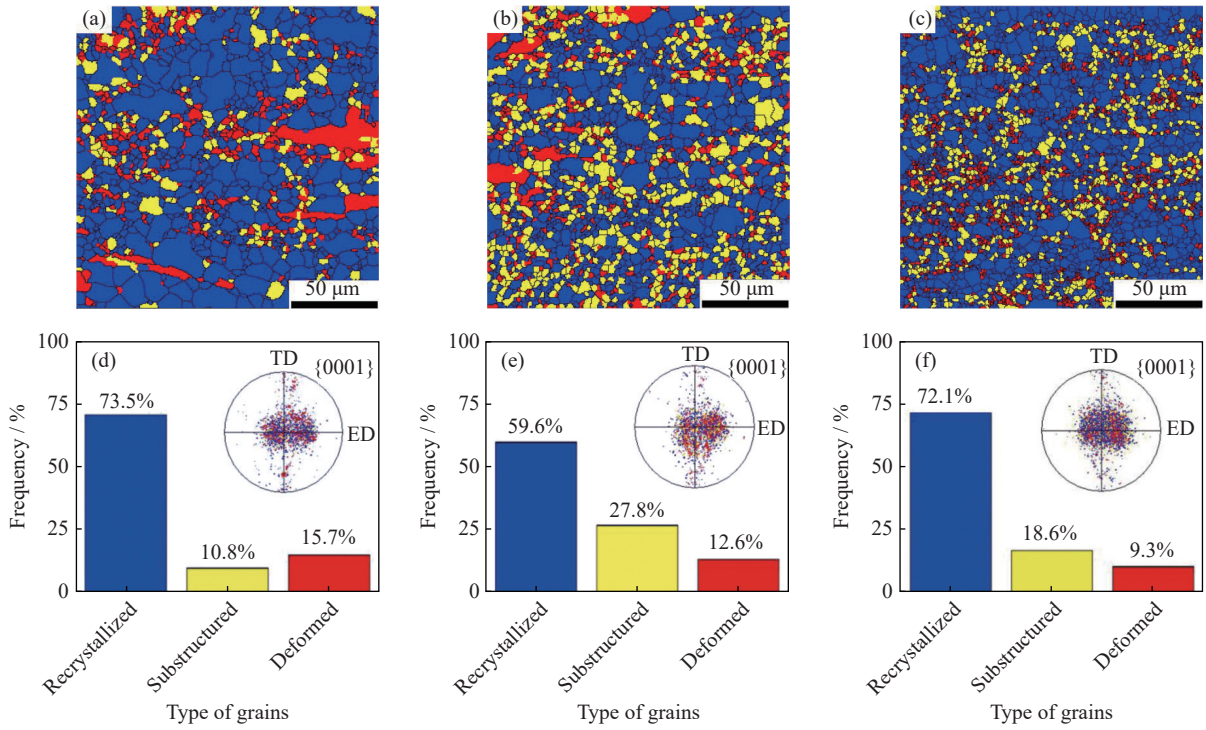

Fig. 7. Different types of grains of (a) CE sheet, (b) SE1 sheet, and (c) SE2 sheet: blue—recrystallized, yellow—substructured, and red—deformed; (d), (e), and (f) frequency and corresponding (0001) pole figures of the different types of grains shown in (a), (b), and (c), respectively.

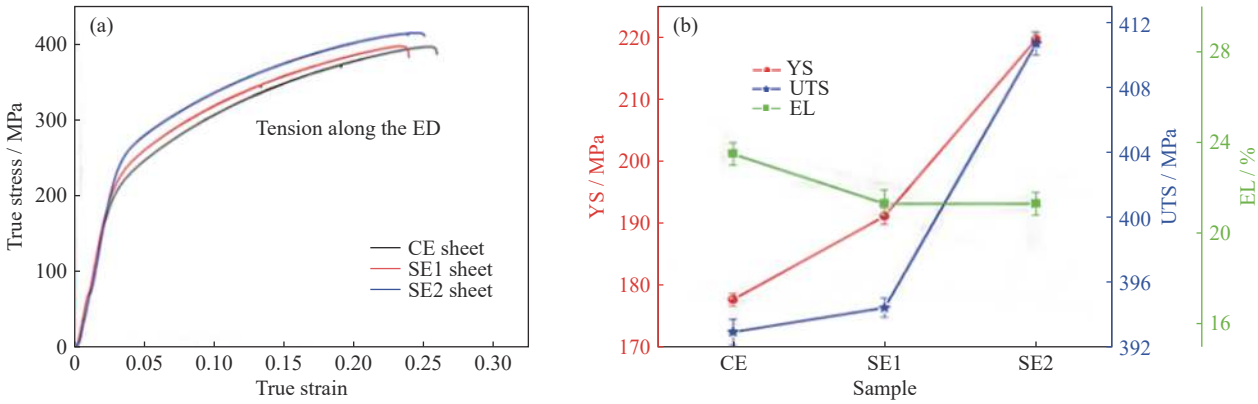

Fig. 8. (a) True stress–true strain curves of the sample CE, SE1, and SE2; (b) average values for yield strength (YS) and ultimate tensile strength (UTS), and elongation-to-failure (EL) for the CE, SE1, and SE2 sheets.

texture intensity [27]), and τ_0 is the resolved shear stress for glide on the easiest slip system (about 1.0 MPa [28]). By using the data of average grain size (CE: 9.1 μm; SE1: 7.7 μm; SE2: 5.6 μm), the calculated YS of as-extruded alloys is 154.8, 193.7, and 219.7 MPa, respectively, which has a good correspondence with their actual values. Hence, the above increase in strength values induced by the SE processes can be attributed to grain refinement and basal texture enhancement. Similarly, research of Ding *et al.* [29] revealed that the increased strength of the billet by procedure 10-ACB can be attributed to the effects of submicron-grained structure and texture strengthening.

The EL values of SE1 and SE2 sheets present a slight decrease (21.1% and 21.3 %, respectively) compared with the CE sheet (23.5%). The main factors affecting the ductility of alloys are summarized as follows: (1) Grain size. Generally speaking, with the decrease of grain size, the strain difference between grain internal and grain boundary becomes smaller under the condition of same external force [30]. In other words, grain refinement can reduce the cracking induced by stress concentration and result in more uniform deformation [31]. Hence, refined grains are in favor of enhancing the ductility of the Mg alloys [32–33]. (2) Texture. As well known, conventional hot rolling often produces a strong basal texture in Mg alloy sheets, and which will inevitably deteriorate the ductility, due to the lack of an effective deformation mechanism to coordinate the strain along the thickness direction [34–35].

Fig. 9 demonstrates the Schmid factors (SF) for (0002) $\langle 11\bar{2}0 \rangle$ basal slip of AZ31 alloys fabricated by three different extrusion processes. In general, SF indicates the feasibility and activation degree of a certain slip mode regarding the loading direction [36–38]. In the present study, the higher

value of average SF implies the easier activation of basal slip and consequently the lower YS just from the perspective of texture. On the basis of the similar average value of basal slip SF among these three different extrusion processes (CE: 0.243; SE1: 0.267; SE2: 0.244), it can be figured out that the activation of basal slip in the CE and SE processes is analogous. In conclusion, the excellent ductility of SE sheets at room temperature can be attributed to the fact that the positive effect from refined grains offsets the deteriorating effect from the intense basal texture.

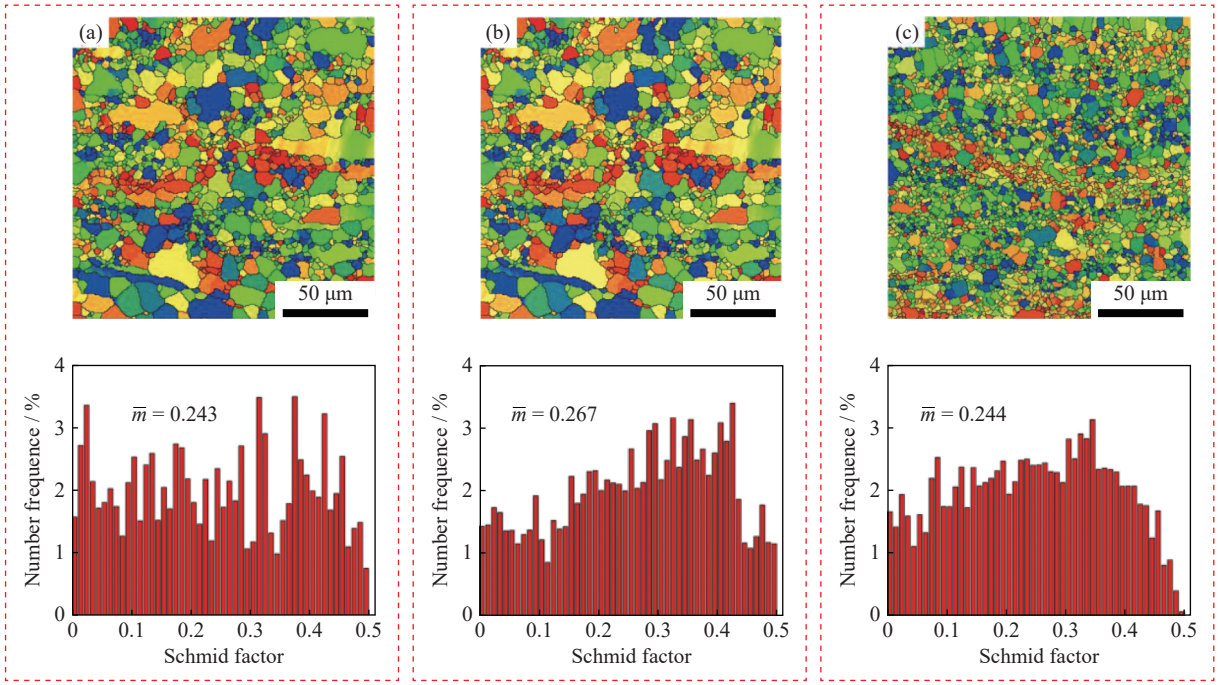

Fig. 9. Schmid factors for (0002)⟨11$\bar{2}$0⟩ basal slip of the samples (a) CE, (b) SE1, and (c) SE2 during tension along the ED. $\bar{m}$ is the average value for the corresponding Schmid factor.

4. Conclusions

The SE was carried out to produce the AZ31 sheet. The microstructures, textures, and mechanical properties at room temperature were examined. The conclusions were drawn as follows.

(1) Additional introduced inclined interface in the slope extrusion process could bring about more asymmetric deformation and stronger accumulated strain along the ND.

(2) The increment of normal strain during slope extrusion could bring about grain refinement, reasonable texture enhancement, and the improvement of microstructural homogeneity.

(3) The increased YS and UTS of SE sheets were associated with the synergistic effects from grain refinement and texture strengthening. Besides, excellent ductility of SE sheets was pertained to the positive effect from refined grains.

Therefore, the SE process was a simple and effective method to enhance the strength of Mg alloy sheet.

Acknowledgements

This work was financially supported by the National Natural Science Foundation of China (Nos. U1764253, 51971044, 51901204, U1910213 52001037, and U207601), the National Defense Basic Scientific Research Program of China, the Chongqing Science and Technology Commission, China (No. cstc2017zdcy-zdzxX0006), the Chongqing Municipal Education Commission, China (No. KJZD-K202001502), the Chongqing Scientific & Technological Talents Program, China (No. KJXX2017002), the Qinghai Scientific & Technological Program, China (No. 2018-GX-A1), the Zhejiang Provincial Natural Science Foundation, China (No. LGG21E050009), and the Research Start-up Funds of Shaoxing University, China (No. 20210007).

Conflict of Interest

The authors declare no conflict of interest.

References

[1] J.F. Song, J. She, D.L. Chen, and F.S. Pan, Latest research advances on magnesium and magnesium alloys worldwide, *J. Magnes. Alloys*, 8(2020), No. 1, p. 1.

[2] Q.S. Yang, Q.W. Dai, C. Lou, J.H. Dai, J.Y. Zhang, B. Jiang, and F.S. Pan, Twinning, grain orientation, and texture variations in Mg alloy processed by pre-rolling, *Prog. Nat. Sci. Mater. Int.*, 29(2019), No. 2, p. 231.

[3] Q.H. Wang, S.Y. Chen, B. Jiang, Z.Y. Jin, L.Y. Zhao, J.J. He, D.F. Zhang, G.S. Huang, and F.S. Pan, Grain size dependence of annealing strengthening of an extruded Mg–Gd–Zn alloy subjected to pre-compression deformation, *J. Magnes. Alloys*, (2021). DOI: 10.1016/j.jma.2021.03.015

[4] H.H. Yu, Y.C. Xin, M.Y. Wang, and Q. Liu, Hall-Petch rela-

tionship in Mg alloys: A review, *J. Mater. Sci. Technol.*, 34(2018), No. 2, p. 248.
[5] G.Z. Kang and H. Li, Review on cyclic plasticity of magnesium alloys: Experiments and constitutive models, *Int. J. Miner. Metall. Mater.*, 28(2021), No. 4, p. 567.
[6] Q.S. Yang, B. Jiang, B. Song, Z.J. Yu, D.W. He, Y.F. Chai, J.Y. Zhang, and F.S. Pan, The effects of orientation control *via* tension-compression on microstructural evolution and mechanical behavior of AZ31 Mg alloy sheet, *J. Magnes. Alloys*, 10(2022), No. 2, p. 411.
[7] Q. Li, Y.F. Lu, Q. Luo, X.H. Yang, Y. Yang, J. Tan, Z.H. Dong, J. Dang, J.B. Li, Y. Chen, B. Jiang, S.H. Sun, and F.S. Pan, Thermodynamics and kinetics of hydriding and dehydriding reactions in Mg-based hydrogen storage materials, *J. Magnes. Alloys*, 9(2021), No. 6, p. 1922.
[8] Q.H. Wang, B. Jiang, Y.F. Chai, B. Liu, S.X. Ma, J. Xu, and F.S. Pan, Tailoring the textures and mechanical properties of AZ31 alloy sheets using asymmetric composite extrusion, *Mater. Sci. Eng. A*, 673(2016), p. 606.
[9] Q.S. Yang, B. Jiang, G.Y. Zhou, J.H. Dai, and F.S. Pan, Influence of an asymmetric shear deformation on microstructure evolution and mechanical behavior of AZ31 magnesium alloy sheet, *Mater. Sci. Eng. A*, 590(2014), p. 440.
[10] J. Xu, T.H. Yang, B. Jiang, J.F. Song, J.J. He, Q.H. Wang, Y.F. Chai, G.S. Huang, and F.S. Pan, Improved mechanical properties of Mg–3Al–1Zn alloy sheets by optimizing the extrusion die angles: Microstructural and texture evolution, *J. Alloys Compd.*, 762(2018), p. 719.
[11] H.T. Kang and T. Ostrom, Mechanical behavior of cast and forged magnesium alloys and their microstructures, *Mater. Sci. Eng. A*, 490(2008), No. 1-2, p. 52.
[12] T.J. Lee and W.J. Kim, The significant effect of adding trace amounts of Ti on the high-temperature deformation behavior of fine-grained Mg–6Al–1Zn magnesium alloys, *J. Alloys Compd.*, 617(2014), p. 352.
[13] F. Guo, D.F. Zhang, X.S. Yang, L.Y. Jiang, and F.S. Pan, Microstructure and texture evolution of AZ31 magnesium alloy during large strain hot rolling, *Trans. Nonferrous Met. Soc. China*, 25(2015), No. 1, p. 14.
[14] B. Song, R.L. Xin, G. Chen, X.Y. Zhang, and Q. Liu, Improving tensile and compressive properties of magnesium alloy plates by pre-cold rolling, *Scripta Mater.*, 66(2012), No. 12, p. 1061.
[15] W.J. Kim, H.W. Lee, S.J. Yoo, and Y.B. Park, Texture and mechanical properties of ultrafine-grained Mg–3Al–1Zn alloy sheets prepared by high-ratio differential speed rolling, *Mater. Sci. Eng. A*, 528(2011), No. 3, p. 874.
[16] M.T. Pérez-Prado, J.A. del Valle, and O.A. Ruano, Achieving high strength in commercial Mg cast alloys through large strain rolling, *Mater. Lett.*, 59(2005), No. 26, p. 3299.
[17] Y.F. Chai, Y. Song, B. Jiang, J. Fu, Z.T. Jiang, Q.S. Yang, H.R. Sheng, G.S. Huang, D.F. Zhang, and F.S. Pan, Comparison of microstructures and mechanical properties of composite extruded AZ31 sheets, *J. Magnes. Alloys*, 7(2019), No. 4, p. 545.
[18] H.C. Pan, G.W. Qin, Y.M. Huang, Y.P. Ren, X.C. Sha, X.D. Han, Z.Q. Liu, C.F. Li, X.L. Wu, H.W. Chen, C. He, L.J. Chai, Y.Z. Wang, and J.F. Nie, Development of low-alloyed and rare-earth-free magnesium alloys having ultra-high strength, *Acta Mater.*, 149(2018), p. 350.
[19] F.S. Pan, Q.H. Wang, B. Jiang, J.J. He, Y.F. Chai, and J. Xu, An effective approach called the composite extrusion to improve the mechanical properties of AZ31 magnesium alloy sheets, *Mater. Sci. Eng. A*, 655(2016), p. 339.
[20] J.J. He, B. Jiang, H.M. Xie, Z.T. Jiang, B. Liu, and F.S. Pan, Improved tension-compression performance of Mg-Al-Zn alloy processed by co-extrusion, *Mater. Sci. Eng. A*, 675(2016), p. 76.
[21] J. Xu, B. Jiang, J.F. Song, J.J. He, P. Gao, W.J. Liu, T.H. Yang, G.S. Huang, and F.S. Pan, Unusual texture formation in Mg–3Al–1Zn alloy sheets processed by slope extrusion, *Mater. Sci. Eng. A*, 732(2018), p. 1.
[22] L.W. Lu, C.M. Liu, J. Zhao, W.B. Zeng, and Z.C. Wang, Modification of grain refinement and texture in AZ31 Mg alloy by a new plastic deformation method, *J. Alloys Compd.*, 628(2015), p. 130.
[23] Q.S. Yang, B. Jiang, Y. Tian, W.J. Liu, and F.S. Pan, A tilted weak texture processed by an asymmetric extrusion for magnesium alloy sheets, *Mater. Lett.*, 100(2013), p. 29.
[24] D. Wu, W.N. Tang, R.S. Chen, and E.H. Han, Strength enhancement of Mg–3Gd–1Zn alloy by cold rolling, *Trans. Nonferrous Met. Soc. China*, 23(2013), No. 2, p. 301.
[25] Y.F. Chai, B. Jiang, J.F. Song, Q.H. Wang, H. Gao, B. Liu, G.S. Huang, D.F. Zhang, and F.S. Pan, Improvement of mechanical properties and reduction of yield asymmetry of extruded Mg–Sn–Zn alloy through Ca addition, *J. Alloys Compd.*, 782(2019), p. 1076.
[26] T. Hu, W.L. Xiao, F. Wang, Y. Li, S.Y. Lyu, R.X. Zheng, and C.L. Ma, Improving tensile properties of Mg–Sn–Zn magnesium alloy sheets using pre-tension and ageing treatment, *J. Alloys Compd.*, 735(2018), p. 1494.
[27] W.L. Cheng, Q.W. Tian, H. Yu, H. Zhang, and B.S. You, Strengthening mechanisms of indirect-extruded Mg–Sn based alloys at room temperature, *J. Magnes. Alloys*, 2(2014), No. 4, p. 299.
[28] B.Q. Shi, R.S. Chen, and W. Ke, Solid solution strengthening in polycrystals of Mg–Sn binary alloys, *J. Alloys Compd.*, 509(2011), No. 7, p. 3357.
[29] S.X. Ding, W.T. Lee, C.P. Chang, L.W. Chang, and P.W. Kao, Improvement of strength of magnesium alloy processed by equal channel angular extrusion, *Scripta. Mater.*, 59(2008), No. 9, p. 1006.
[30] J.B. Liu, K. Zhang, J.T. Han, X.G. Li, Y.J. Li, M.L. Ma, J.W. Yuan, and G.L. Shi, Microstructure and texture evolution of Mg–7Y–1Nd–0.5Zr alloy sheets with different rolling temperatures, *Rare Met.*, 39(2020), No. 11, p. 1273.
[31] K. Liu, J.T. Liang, W.B. Du, S.B. Li, Z.H. Wang, Z.J. Yu, and J.X. Liu, Microstructure, mechanical properties and stretch formability of as-rolled Mg alloys with Zn and Er additions, *Rare Met.*, 40(2021), No. 8, p. 2179.
[32] L.L. Chang, J.H. Cho, and S.K. Kang, Microstructure and mechanical properties of twin roll cast AM31 magnesium alloy sheet processed by differential speed rolling, *Mater. Des.*, 34(2012), p. 746.
[33] J. Zhao, B. Jiang, Q.H. Wang, M. Yuan, Y.F. Chai, G.S. Huang, and F.S. Pan, Effects of Li addition on the microstructure and tensile properties of the extruded Mg–1Zn–*x*Li alloy, *Int. J. Miner. Metall. Mater.*, 29(2022), No. 7, p. 1380.
[34] Q.W. Dai, D.F. Zhang, and X. Chen, On the anisotropic deformation of AZ31 Mg alloy under compression, *Mater. Des.*, 32(2011), No. 10, p. 5004.
[35] Q.H. Wang, B. Jiang, A.T. Tang, S.X. Ma, Z.T. Jiang, Y.F. Chai, B. Liu, and F.S. Pan, Ameliorating the mechanical properties of magnesium alloy: Role of texture, *Mater. Sci. Eng. A*, 689(2017), p. 395.
[36] C. He, Y.B. Zhang, M. Yuan, B. Jiang, Q.H. Wang, Y.F. Chai, G.S. Huang, D.F. Zhang, and F.S. Pan, Improving the room-temperature bendability of Mg–3Al–1Zn alloy sheet by introducing a bimodal microstructure and the texture re-orientation, *Int. J. Miner. Metall. Mater.*, 29(2022), No. 7, p. 1322.
[37] Q.H. Wang, B. Jiang, D.L. Chen, Z.Y. Jin, L.Y. Zhao, Q.S. Yang, G.S. Huang, and F.S. Pan, Strategies for enhancing the room-temperature stretch formability of magnesium alloy sheets: A review, *J. Mater. Sci.*, 56(2021), No. 23, p. 12965.
[38] J.F. Song, J. Chen, X.M. Xiong, X.D. Peng, D.L. Chen, and F.S. Pan, Research advances of magnesium and magnesium alloys worldwide in 2021, *J. Magnes. Alloys*, (2022). DOI: 10.1016/j.jma.2022.04.001.